IEEE Photonics Journal
An IEEE Photonics Society Publication

Design of X-Cut and Z-Cut Lithium Niobate Whispering-Gallery-Mode Disk-Resonators With High Quality Factors

Volume 9, Number 4, August 2017

Yu Pan
Guoping Lin
Souleymane Diallo
Xianmin Zhang
Yanne K. Chembo, ***Senior Member, IEEE***

DOI: 10.1109/JPHOT.2017.2727286
1943-0655 © 2017 IEEE

IEEE photonics SOCIETY

IEEE

Design of X-Cut and Z-Cut Lithium Niobate Whispering-Gallery-Mode Disk-Resonators With High Quality Factors

Yu Pan,[1,2] Guoping Lin,[1,3] Souleymane Diallo,[1] Xianmin Zhang,[2] and Yanne K. Chembo,[1,4] *Senior Member, IEEE*

[1]Optics Department, FEMTO-ST Institute, CNRS, University Bourgogne Franche-Comté, Besançon 25030, France
[2]College of Information Science and Electronic Engineering, Zhejiang University, Hangzhou 310027, China
[3]MOE Key Laboratory of Fundamental Physical Quantities Measurement, School of Physics, Huazhong University of Science and Technology, Wuhan 430074, China
[4]Atlanta Mirror Site, and the School of Electrical and Computer Engineering, GeorgiaTech-CNRS Joint International Laboratory [UMI 2958], Atlanta, GA 30332-0250 USA

DOI:10.1109/JPHOT.2017.2727286

Manuscript received May 25, 2017; accepted July 10, 2017. Date of publication July 25, 2017; date of current version August 15, 2017. This work was supported in part by the European Research Council under Projects StG NextPhase and PoC Versyt, in part by the Centre National d'Etudes Spatiales under Project SHYRO, in part by the project CORPS (Région de Franche-Comté), in part by the project SYOCUS of the University Bourgogne Franche-Comté, and in part by the Labex ACTION. The work of Y. Pan was supported by the China Scholarship Council under Grant 201506320092. Corresponding author: Yanne K. Chembo (e-mail: yanne.chembo@femto-st.fr).

Abstract: We demonstrate the fabrication process of millimeter-size lithium niobate ($LiNbO_3$) whispering-gallery-mode (WGM) disk-resonators. We fabricate both *x*- and *z*-cut disk-resonators, starting from commercially available $LiNbO_3$ disks with diameters of 12 mm and thicknesses of 1 mm. We characterize these two WGM resonators using a prism coupling configuration. We find that both resonators feature high loaded quality factors, in both cases higher than 10^7 at 1550 nm. We also investigate the polarization and thermal effects in these disk-resonators. The design of high-Q $LiNbO_3$ disk-resonators with different orientations using the same platform will allow for a wide variety of potential applications in nonlinear and quantum photonics.

Index Terms: Disk-resonator, lithium niobate, high-Q factors, whispering-gallery-mode.

1. Introduction

Optical whispering gallery modes (WGMs) are electromagnetic modes confined in circular dielectric resonators, where light beams are guided along the circumference of the resonators by total internal reflection. Among these WGM resonators, mm-size disk-resonators have attracted great attention in recent years. Their quality (Q) factors can reach significantly high values, close to the material absorption limit, resulting in exceptionally long photon lifetimes (up to few tens of μs) in strongly confined modes. This excellent feature allows for a wide range of applications such as lasing, sensing, time-frequency metrology, as well as lightwave and microwave technology [1]–[7].

Mechanical polishing techniques provide an efficient method to fabricate WGM disk-resonators with various host materials, such as calcium fluoride [8]–[11], magnesium fluoride [12]–[18], barium fluoride [19]–[21], strontium fluoride [22], lithium fluoride [23], or even diamond [24], [25], amongst other crystals. In particular, lithium niobate ($LiNbO_3$) has been successfully used to fabricate WGM disk-resonators, leading to numerous applications in optics and microwave photonics, such as electro-optic modulators, photonic microwave receivers, tunable optical filters, second harmonic generation, etc. (see [26]–[39] and references therein). However, it is still a difficult task to fabricate high Q resonators by mechanical polishing. On the one hand, the fabrication of $LiNbO_3$ disk-resonators usually requires much efforts and time because of its high hardness. On the other hand, it is not easy to achieve a very high Q factor due to the limitation of the relatively high absorption loss for this material.

In this paper, we report the fabrication process of high Q $LiNbO_3$ WGM disk-resonators in both the x- and z-cut orientations. Our disks have a diameter of 12 mm and a thickness of 1 mm. To the best of our knowledge, this is the first time that an high Q mm-size x-cut $LiNbO_3$ disk-resonator is demonstrated. We characterize these two disk-resonators using a prism coupling experimental setup, and both of them are demonstrated to feature high Q factors ($>10^7$). Our disk-resonators also show different coupling efficiencies under different polarization states. Furthermore, we study in detail thermal effects in the x-cut $LiNbO_3$ disk-resonator, and present the time evolution of WGM resonances. It should be noted that TM modes in an x-cut $LiNbO_3$ disk-resonator experience varying refractive index and nonlinear coefficient along the circumference. This unique feature, together with its high Q factor and excellent electro-optic effect, enables various potential applications of $LiNbO_3$ WGM disk-resonators in optics and microwave photonics.

The outline of the article is the following. In the next section, we describe in detail the fabrication process of the resonators. Then, we present the experimental setup used to pump them, and we explore the sensitivity of the coupling with the input polarization. Section 4 is devoted to investigations related to the Q-factor of the x-and z-cut resonators, as well as their sensitivity with input polarization and pump-induced temperature shifts. The last section concludes the article.

2. Fabrication Process

The WGM resonators were fabricated using commercially available $LiNbO_3$ disks with diameters of 12 mm and thicknesses of 1 mm. The disks were provided by Korth Krystalle GMBH. As the Q-factor of a WGM resonator depends in part on its surface roughness, the rim of the disk should be very smooth to allow for a high Q factor. The aim of the fabrication process is to reduce the surface roughness to the smallest value possible. An air-bearing spindle motor was used to spin the disk, and different powders were used to reduce the roughness of the surface rim [40]. In general, the fabrication is divided into three steps: grinding, smoothing and polishing. In the grinding stage, wood supports covered with oil-mixed abrasive powders (29 μm and 9 μm, respectively) were brought in soft contact to the spinning disk. The rim of the disk was therefore gradually modified and led to converge to a V-shape during this process. In the smoothing process, tissues covered with mixtures of abrasive particles (6 μm and 3 μm) were used to remove the scratches and stripes caused by the grinding process. Due to the high hardness of $LiNbO_3$, this process would usually take much more time, and a shining rim could be observed in the microscope at the end of this process. Finally we went to the polishing process, where much smaller mixtures of abrasive particles (1 μm) were used to polish the rim. The surface roughness would be further reduced and a very smooth and shining rim surface could be observed in the microscope at the end of this process. When the three steps were performed, the disk-resonator was expected to have a high Q factor, as it can be seen in Fig. 1 where our resonators are coupled in the red. We have fabricated both z-cut and x-cut high Q $LiNbO_3$ disk-resonators using this technique.

3. Experimental Setup

The schematic representation of the experimental setup for the high Q $LiNbO_3$ WGM disk-resonators is shown in Fig. 2. A tunable continuous wave (cw) laser with sub-kHz instantaneous

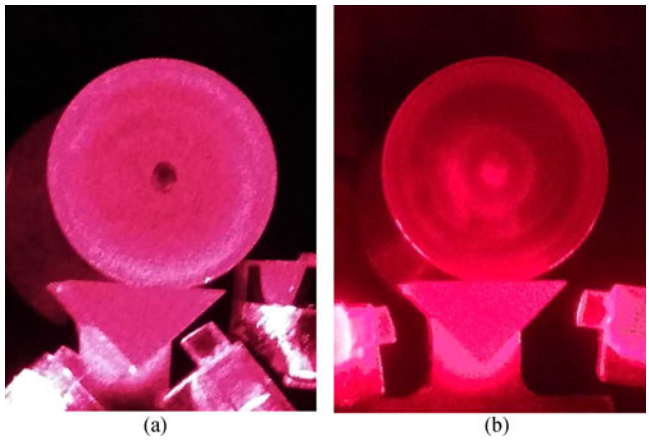

Fig. 1. Pictures of the polished $LiNbO_3$ disk-resonators coupled using a rutile prism. (a) *z*-cut resonator. (b) *x*-cut resonator.

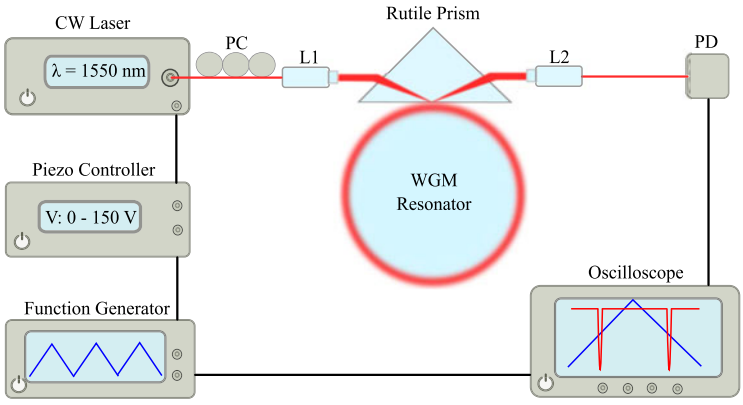

Fig. 2. Schematic representation of the experimental setup for the high *Q* $LiNbO_3$ WGM disk-resonators. PC: polarization controller; L1 and L2: gradient-index (GRIN) lens; PD: photodetector. The piezo-controller is used to scan the frequency of the laser.

linewidth is used to excite WGM resonances in the disk-resonators, when the laser wavelength is scanned near 1550 nm using a piezo-driver controlled by a function generator. The polarization state of the laser beam is adjusted with a fiber polarization controller (PC). The first pigtailed gradient-index (GRIN) lens (L1) focuses the incident beam on the interface of the prism for WGM coupling, and the second one (L2) collects the output beam into a single-mode optical fiber. Then the output is detected by a photodetector (PD) and monitored with a high resolution digital oscilloscope (InfiniiVision DSO-X 2014A, 100 MHz bandwidth and 2 GSa/s acquisition).

Because of the high refractive indices of $LiNbO_3$ ($n_e = 2.138$ at 1550 nm for *z*-cut $LiNbO_3$), we use a rutile prism with higher refractive indices ($n_e = 2.694$ at 1550 nm) to couple the laser beam into the disk, as displayed in Fig. 2. The prism coupling is realized through frustrated total internal reflection, where the incident angle should be chosen to fulfill the condition of the total internal reflection. We choose different incident angles for the *z*-cut and *x*-cut coupling, since the effective refractive indices of *z*-cut and *x*-cut $LiNbO_3$ resonators could be different depending on the beam polarization state and relative coupling position. It should be noted that when light is coupled to a lithium niobate resonator using a rutile prism, only one polarization at a time can be coupled because of the difference between ordinary and extraordinary indices in rutile and lithium niobate. However, both polarizations can be coupled simultaneously using a lithium niobate coupler [41].

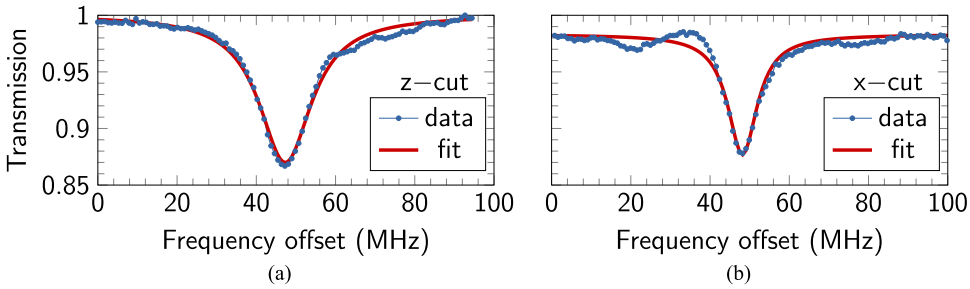

Fig. 3. Normalized transmission spectra of WGM resonances for the *x*-and*z*-cut $LiNbO_3$ disk-resonators, along with their Lorentzian fit. (a) *z*-cut WGM resonator. The full width at half maximum of the Lorentzian fit is $\Delta f = 16.2$ MHz, yielding a loaded Q factor of 1.2×10^7. (b) *x*-cut WGM resonator. The full width at half maximum of the Lorentzian fit is $\Delta f = 10.9$ MHz, yielding a loaded Q factor of 1.8×10^7.

A three-dimensional stage is also used to finely control the gap between the prism and resonator, which should be within the skin depth of the evanescent wave.

4. Results and Discussions

4.1 Z-Cut $LiNbO_3$ Disk-Resonator

We first investigate the *z*-cut $LiNbO_3$ disk-resonator. When the gap between the prism and disk is sufficiently small, WGM resonances could be excited in the disk-resonator, and several transmission dips can be observed in the oscilloscope. Fig. 3(a) shows one of the dips when the laser is scanned around one WGM resonance. The transmission dip is fitted with a Lorentzian line shape to evaluate the Q-factor of the disk-resonator. The full width at half maximum (FWHM) of the Lorentzian fit is $\Delta f = 16.2$ MHz, yielding a Q factor of 1.2×10^7. In addition, the small dip contrast of Fig. 3(a) suggests that the disk-resonator could be in the under-coupling regime, where only a small fraction of the laser power is coupled into and out of the disk-resonator, resulting in a very low coupling loss. Such small dips could also result from a non-optimal coupling angle. Generally, the quality factor Q can be expressed as $Q^{-1} = Q_m^{-1} + Q_c^{-1} + Q_s^{-1} + Q_r^{-1}$, where Q_m^{-1} is the material absorption loss, Q_c^{-1} is the coupling loss, Q_s^{-1} is the surface scattering loss, and Q_r^{-1} is the radiation loss. The surface scattering loss Q_s^{-1} and radiation loss Q_r^{-1} are negligible in our case, and the coupling loss Q_c^{-1} is also very small when the disk-resonator is under-coupled. Therefore the Q factor of this *z*-cut $LiNbO_3$ disk-resonator could be mainly limited by the high material absorption loss of $LiNbO_3$.

It is noteworthy that this coupling system is very sensitive to the polarization state of the laser beam, due to the birefringences of the rutile prism and the $LiNbO_3$ resonator. Under different polarization states, the transmission and reflection directions of the laser beams are slightly different, resulting in different WGM coupling efficiencies. One should also note that the WGM resonance is polarization-dependant. In order to achieve a maximum coupling efficiency, the polarization state of the input beam should be adjusted to match with the one of WGM resonances. Fig. 4(a) shows the transmission spectra obtained under different polarization states. It can be seen that the same group of WGM resonances shown in different colors are excited in the resonator, when the laser beams are in different polarization states. However, these resonances experience different coupling efficiencies as a result of polarization mismatch. The blue curve shows the maximum dip contrast, suggesting that a maximum coupling efficiency is achieved at the corresponding polarization state.

4.2 X-Cut $LiNbO_3$ Disk-Resonator

Now we consider the case of the *x*-cut $LiNbO_3$ disk-resonator. An interesting characteristic of the *x*-cut $LiNbO_3$ disk-resonator is that TM modes experience varying refractive index and nonlinear coefficient along the circumference, leading to potential applications in nonlinear optics such as

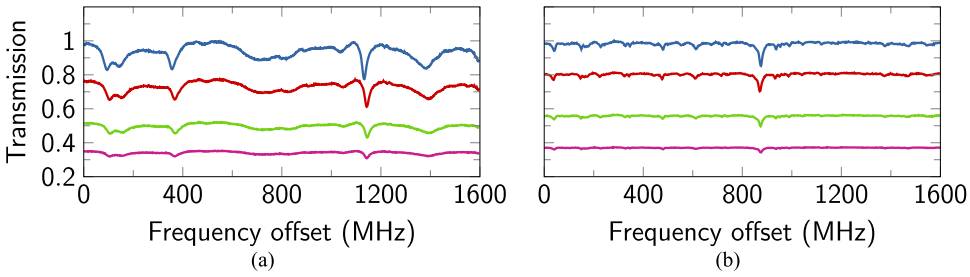

Fig. 4. Transmission spectra obtained under different polarization states when the laser is scanned around a group of WGM resonances, with different color representing different polarization states. (a) *z*-cut WGM resonator; (b) *x*-cut WGM resonator.

parametric oscillations or second harmonic generation [42]–[47]. We are able to measure the Q factor of this *x*-cut disk-resonator using the same experimental setup of Fig. 2. However, the incident angle of the laser beam should be adjusted specially to fulfill the phase matching condition for TM-polarized WGM excitation that is dependent on the relative position of the *x*-cut disk. As shown in Fig. 3(a), high-Q resonances can be excited as well in these resonators. The minimum linewidth is 10.9 MHz, yielding a Q-factor of 1.8×10^7. This quality factor is higher than that of the *z*-cut resonator, suggesting lower optical losses in the *x*-cut resonator. The polarization dependence for this resonator is displayed in Fig. 4(b).

We also investigate thermal effects in our WGM resonators. WGMs would usually experience temperature change when the laser is coupled into the resonator, giving rise to a wide variety of complex phenomena, including thermal relaxation oscillations [48], [49]. For a WGM resonator, the temperature dependence of a resonance of wavelength λ_0 can be expressed as $\lambda_0 = (2\pi/\ell_0)\, n_{\text{eff}}(T_1) R_{\text{eff}}(T_2)$, where $n_{\text{eff}}(T_1)$ is the effective refractive index, $R_{\text{eff}}(T_2)$ is the effective radius of the resonator, and ℓ_0 is the mode number, T_1 and T_2 are respectively the temperatures of the mode area and the overall resonator. It should be noted that both $n_{\text{eff}}(T_1)$ and $R_{\text{eff}}(T_2)$ are temperature dependent. When the laser is repeatedly coupled into the resonator and consequently heats it, temperatures of T_1 and T_2 will keep increasing, resulting in the changing of $n_{\text{eff}}(T_1)$ and $R_{\text{eff}}(T_2)$, and eventually causing the wavelength shift. This wavelength shift could be expressed as: $\Delta\lambda_0/\lambda_0 = \alpha_1 \Delta T_1(t) + \alpha_2 \Delta T_2(t)$, where $\Delta\lambda_0$ is the wavelength shift caused by thermal effects, $\Delta T_1(t)$ and $\Delta T_2(t)$ are respectively the temperature changes of the mode area and the overall resonator, and $\alpha_{1,2}$ are the corresponding thermal coefficients. The first term in the right-hand side represents the thermo-optic effect, corresponding to fast time-scale thermal transfers, and the second term represents the thermal expansion effect, which is generally much slower, since it takes much more time for the heat to diffuse from the mode volume to the full volume of resonator.

Previous research has evidenced photo-refractivity in lithium niobate (see for example [50], [51]). We have followed the resonance drift dynamics in a minute-timescale in Fig. 5. We switch on the laser (with 35 mW continuous-wave power) to heat the resonator and switch off to cool it. The data are recorded every minute when the laser is continuously coupled into the *x*-cut $LiNbO_3$ disk resonator, except that there are 30 seconds of natural cooling by turning the laser off, before the measurement at the third minute. We take the first measurement when the laser is on, as shown in timetrace at 0 min in Fig. 5, and the second and third measurements are taken after the laser is switched on for 1 minute and 2 minutes. Then we turn the laser off, let the resonator cool for 30 seconds. The laser is turned on again, and we take the fourth and fifth measurements at the third and fourth minutes, as shown in Fig. 5. One can see from the resonance at 1, 2 and 4 min, that the WGM resonance is red-shifted when the laser is continuously coupled to the resonator, which is thereby heated. Due to the 30 s-cooling when the laser is switched off, the WGM resonance at 3 min is shifted back to the position of 0 min. This difference in frequency shift direction between the laser on and off states confirms the reversibility of the thermal effects in the resonator.

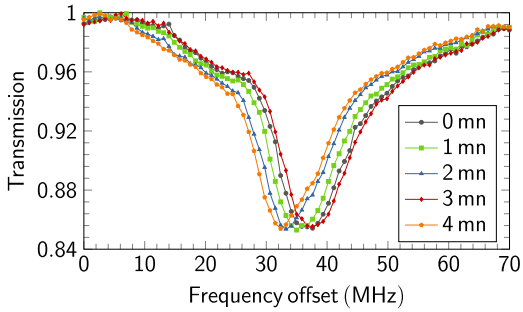

Fig. 5. Temporal drift of the WGM resonances in the *x*-cut $LiNbO_3$ disk resonator. The data is recorded every minute when the laser is continuously coupled into the resonator, except that there are 30 seconds of natural cooling by turning the laser off, just before the measurement at the third minute.

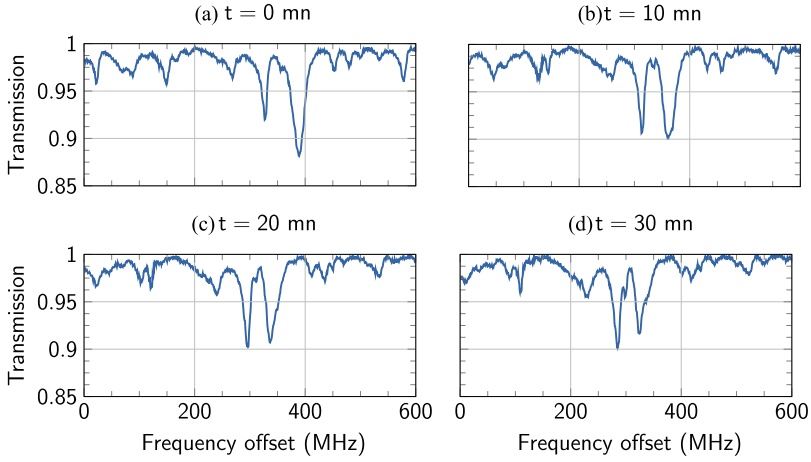

Fig. 6. Time evolution of WGM resonances in the *x*-cut $LiNbO_3$ disk-resonator, recorded every 10 minutes when the laser is continuously coupled into the resonator.

Fig. 6 shows the time evolution of WGM resonances in the *x*-cut $LiNbO_3$ disk-resonator, where two WGM resonances are recorded every 10 minutes when the laser is continuously coupled into the resonator. As a result of laser heating, temperatures of the mode volume and disk-resonator would keep increasing. Both the thermo-optic and thermal expansion coefficients $\alpha_{1,2}$ for $LiNbO_3$ are positive, therefore the two WGM resonances are shifted to longer wavelengths by the positive thermo-optic effect and positive thermal expansion effect, as can be seen in Fig. 6. We find that the wavelength of the left WGM resonance is shifted by $\sim$60 MHz by thermal effects in 30 minutes. In addition to the redshift of WGM resonances, one can see the mode competition between these two WGM resonances. At the beginning, the left WGM resonance is the dominant mode in the resonator [see Fig. 6(a)]. As the coupling time increasing, the dip contrast keeps decreasing for the left resonance while it keeps growing for the right one [see Fig. 6(b) and (c)]. As the coupling time keeps increasing, the right resonance eventually becomes the dominant mode [see Fig. 6(d)]. This mode competition which is powered by the temperature change of the resonator is an indication of the complex thermal dynamics in these resonators.

5. Conclusion

We have reported the fabrication process of mm-size $LiNbO_3$ WGM disk-resonators in both the *x*- and *z*-cut orientations using the same platform. We have used a rutile prism to couple the

laser beam into the disk-resonators and then evaluated the Q factors of the two disk-resonators, which were found to be higher than ten millions. Furthermore, we have studied in the influence of input polarization and thermal load in the disk-resonator. The second order nonlinearities of these high-Q resonators offer unique possibilities for many potential applications in optics and microwave photonics. Future research will consider further increasing of the Q-factors of our resonators (such as in [52]) in order to implement optical filters for time-frequency metrology applications [53], [54]. We will also investigate competing nonlinearities in such resonators [55], [56], as well as the quantum properties of the intracavity fields [6], [57], [58].

Acknowledgment

Y. Pan would like to thank the FEMTO-ST Institute for the completion of this research work.

References

[1] A. B. Matsko and V. S. Ilchenko, "Optical resonators with whispering gallery modes I: Basics," *IEEE J. Sel. Topics Quantum Electron.*, vol. 12, no. 1, pp. 3–14, Jan./Feb. 2006.
[2] V. S. Ilchenko and A. B. Matsko, "Optical resonators with whispering-gallery modes–part II: Applications," *IEEE J. Sel. Topics Quantum Electron.*, vol. 12, no. 1, pp. 15–32, Jan./Feb. 2006.
[3] A. Chiasera *et al.*, "Spherical whispering-gallery-mode microresonators," *Laser Photon. Rev.*, vol. 4, pp. 457–482, 2010.
[4] M. R. Foreman, J. D. Swaim, and F. Vollmer, "Whispering gallery mode sensors," *Adv. Opt. Photon.*, vol. 7, pp. 168–240, 2015.
[5] Y. K. Chembo, "Kerr optical frequency combs: Theory, applications and perspectives," *Nanophotonics*, vol. 5, pp. 214–230, 2016.
[6] D. V. Strekalov, C. Marquardt, A. B. Matsko, H. G. L. Schwefel, and G. Leuchs, "Nonlinear and quantum optics with whispering gallery resonators," *J. Opt.*, vol. 18, 2016, Art. no. 123002.
[7] I. Breunig, "Three-wave mixing in whispering gallery resonators," *Laser Photon. Rev.*, vol. 10, pp. 569–587, 2016.
[8] I. S. Grudinin and L. Maleki, "Ultralow-threshold raman lasing with CaF_2 resonators," *Opt. Lett.*, vol. 32, no. 2, pp. 166–168, 2007.
[9] I. S. Grudinin *et al.*, "Ultra high Q crystalline microcavities," *Opt. Commun.*, vol. 265, pp. 33–38, 2006.
[10] K. Saleh, G. Lin, and Y. K. Chembo, "Effect of laser coupling and active stabilization on the phase noise performance of optoelectronic microwave oscillators based on whispering gallery mode resonators," *IEEE Photon. J.*, vol. 7, no. 1, Feb. 2015, Art. no. 5500111.
[11] K. Saleh and Y. K. Chembo, "Phase noise performance comparison between microwaves generated with Kerr optical frequency combs and optoelectronic oscillators," *Electron. Lett.*, vol. 53, pp. 264–266, 2017.
[12] H. Tavernier, P. Salzenstein, K. Volyanskiy, Y. K. Chembo, and L. Larger, "Magnesium fluoride whispering gallery mode disk-resonators for microwave photonics applications," *IEEE Photon. Tech. Lett.*, vol. 22, no. 22, pp. 1629–1631, Nov. 2010.
[13] D. V. Strekalov, R. J. Thompson, L. M. Baumgartel, I. S. Grudinin, and N. Yu, "Temperature measurement and stabilization in a birefringent whispering gallery mode resonator," *Opt. Exp.*, vol. 19, pp. 14495–14501, 2011.
[14] F. Sedlmeir, R. Zeltner, G. Leuchs, and H. G. L. Schwefel, "High-Q MgF_2 whispering gallery mode resonators for refractometric sensing in aqueous environment," *Opt. Exp.*, vol. 22, pp. 30934–30942, 2014.
[15] A. Coillet and Y. K. Chembo, "Routes to spatiotemporal chaos in Kerr optical frequency combs," *Chaos*, vol. 24, 2014, Art. no. 013113.
[16] W. Weng, J. D. Anstie, and A. N. Luiten, "Refractometry with ultralow detection limit using anisotropic whispering-gallery-mode resonators," *Phys. Rev. Appl.*, vol. 3, 2015, Art. no. 44015.
[17] K. Saleh and Y. K. Chembo, "On the phase noise performance of microwave and millimeter-wave signals generated with versatile Kerr optical frequency combs," *Opt. Exp.*, vol. 24, pp. 25043–25056, 2016.
[18] K. Saleh and Y. K. Chembo, "Optimization of close-in phase noise for microwaves generated with Kerr combs using brillouin-assisted pump depletion," *IEEE Photon. J.*, vol. 8, no. 6, Dec. 2016, Art. no. 5501807.
[19] G. Lin and Y. K. Chembo, "On the dispersion management of fluorite whispering-gallery mode resonators for Kerr optical frequency comb generation in the telecom and mid-infrared range," *Opt. Exp.*, vol. 23, pp. 1594–1604, 2015.
[20] G. Lin *et al.*, "Cascaded Brillouin lasing in monolithic barium fluoride whispering gallery mode resonators," *Appl. Phys. Lett.*, vol. 105, 2014, Art. no. 231103.
[21] G. Lin and Y. K. Chembo, "Phase-locking transition in Raman combs generated with whispering gallery mode resonators," *Opt. Lett.*, vol. 41, pp. 3718–3721, 2016.
[22] R. Henriet *et al.*, "Kerr optical frequency comb generation in strontium fluoride whispering-gallery mode resonators with billion quality factor," *Opt. Lett.*, vol. 40, pp. 1567–1570, 2015.
[23] S. Diallo, G. Lin, R. Martinenghi, L. Furfaro, M. Jacquot, and Y. K. Chembo, "Brillouin lasing in ultra-high-Q lithium fluoride disk resonators," *IEEE Photon. Technol. Lett.*, vol. 28, no. 9, pp. 955–958, May 2016.
[24] V. S. Ilchenko, A. M. Bennett, P. Santini, A. A. Savchenkov, A. B. Matsko, and L. Maleki, "Whispering gallery mode diamond resonator," *Opt. Lett.*, vol. 38, no. 21, pp. 4320–4323, 2013.
[25] B. J. M. Hausmann, I. Bulu, V. Venkataraman, P. Deotare, and M. Loncar, "Diamond nonlinear photonics," *Nature Photon.*, vol. 8, pp. 369–374, 2014.

[26] D. Cohen, M. Hossein-Zadeh, and A. Levi, "High-Q microphotonic electro-optic modulator," *Solid-State Electron.*, vol. 45, pp. 1577–1589, 2001.
[27] M. Hossein-Zadeh and A. Levi, "Mb/s data transmission over a RF fiber-optic link using a $LiNbO_3$ microdisk modulator," *Solid-State Electron.*, vol. 46, pp. 2173–2178, 2002.
[28] A. A. Savchenkov, V. S. Ilchenko, A. B. Matsko, and L. Maleki, "Tunable filter based on whispering gallery modes," *Electron. Lett.*, vol. 39, pp. 389–391, 2003.
[29] A. A. Savchenkov, V. S. Ilchenko, A. B. Matsko, and L. Maleki, "High-order tunable filters based on a chain of coupled crystalline whispering gallery-mode resonators," *IEEE Photon. Technol. Lett.*, vol. 17, no. 1, pp. 136–138, Jan. 2005.
[30] M. Hossein-Zadeh and A. Levi, "Self-homodyne RF-optical $LiNbO_3$ microdisk receiver," *Solid-State Electron.*, vol. 49, pp. 1428–1434, 2005.
[31] M. Mohageg, A. Savchenkov, and L. Maleki, "Coherent backscattering in lithium niobate whispering-gallery-mode resonators," *Opt. Lett.*, vol. 32, pp. 2574–2576, 2007.
[32] V. S. Ilchenko, A. B. Matsko, I. Solomatine, A. A. Savchenkov, D. Seidel, and L. Maleki, "K_a-band all-resonant photonic microwave receiver," *IEEE Photon. Technol. Lett.*, vol. 20, no. 19, pp. 1600–1612, Oct. 2008.
[33] J. U. Furst *et al.*, "Naturally phase-matched second-harmonic generation in a whispering-gallery mode resonator," *Phys. Rev. Lett.*, vol. 104, 2010, Art. no. 153901.
[34] J. U. Furst *et al.*, "Low-threshold optical parametric oscillations in a whispering gallery mode resonator," *Phys. Rev. Lett.*, vol. 105, 2010, Art. no. 263904.
[35] G. Nunzi-Conti *et al.*, "Planar coupling to high-Q lithium niobate disk-resonators," *Opt. Exp.*, vol. 19, pp. 3651–3656, 2011.
[36] L. Maleki and A. B. Matsko, "Lithium niobate whispering gallery Resonators: Applications and fundamental studies," in *Ferroelectric Crystals for Photonic Applications* (Springer Series in Materials Science), vol. 91. Berlin, Germany: Springer, 2014, pp. 337–383.
[37] J. Lin *et al.*, "Fabrication of high-*Q* lithium niobate microresonators using femtosecond laser micromachining," *Sci. Rep.*, vol. 5, 2015, Art. no. 8072.
[38] A. Rueda *et al.*, "Efficient microwave to optical photon conversion: An electro-optical realization," *Optica*, vol. 3, pp. 597–604, 2016.
[39] J. Furst, B. Sturman, K. Buse, and I. Breunig, "Whispering gallery resonators with broken axial symmetry: Theory and experiment," *Opt. Exp.*, vol. 24, pp. 20143–20155, 2016.
[40] A. Coillet *et al.*, "Microwave photonics systems based on whispering-gallery-mode resonators," *J. Vis. Exp.*, vol. 78, 2013, Art. no. e50423.
[41] D. Farnesi *et al.*, "Coupling light to whispering gallery mode resonators," *SPIE Proc.*, vol. 9133, 2014, Art. no. 913314-1.
[42] G. Kozyreff, J. L. Dominguez-Juarez, and J. Martorell, "Nonlinear optics in spheres: From second harmonic scattering to quasi-phase matched generation in whispering gallery modes," *Laser Photon. Rev.* vol. 5, no. 6, pp. 737–749, 2011.
[43] G. Lin, J. Furst, D. V. Strekalov, I. S. Grudinin, and N. Yu, "High-Q UV whispering gallery mode resonators made of angle-cut BBO crystals," *Opt. Exp.*, vol. 20, pp. 21372–21378, 2012.
[44] G. Lin, J. U. Furst, D. V. Strekalov, and N. Yu, "Wide-range cyclic phase matching and second harmonic generation in whispering gallery resonators," *Appl. Phys. Lett.*, vol. 103, 2013, Art. no. 181107.
[45] I. S. Grudinin, G. Lin, and N. Yu, "Polarization conversion loss in birefringent crystalline resonators," *Opt. Lett.*, vol. 38, pp. 2410–2412, 2013.
[46] F. Sedlmeir, M. Hauer, J. U. Furst, G. Leuchs, and H. G. L. Schwefel, "Experimental characterization of an uniaxial angle cut whispering gallery mode resonator," *Opt. Exp.*, vol. 21, pp. 23942–23949, 2013.
[47] F. Leo *et al.*, "Walk-off-induced modulation instability, temporal pattern formation, and frequency comb generation in cavity-enhanced second-harmonic generation," *Phys. Rev. Lett.*, vol. 116, 2016, Art. no. 033901.
[48] A. E. Fomin, M. L. Gorodetsky, I. S. Grudinin, and V. S. Ilchenko, "Nonstationary nonlinear effects in optical microspheres," *J. Opt. Soc. Amer. B*, vol. 22, no. 2, pp. 459–465, 2005.
[49] S. Diallo, G. Lin, and Y. K. Chembo, "Giant thermo-optical relaxation oscillations in millimeter-size whispering gallery mode disk resonators," *Opt. Lett.*, vol. 40, no. 16, pp. 3834–3837, 2015.
[50] A. A. Savchenkov, A. B. Matsko, D. Strekalov, V. S. Ilchenko, and L. Maleki, "Enhancement of photorefraction in whispering gallery mode resonators," *Phys. Rev. B*, vol. 74, 2006, Art. no. 245119.
[51] M. Leidinger, C. S. Werner, W. Yoshiki, K. Buse, and I. Breunig, "Impact of the photorefractive and pyroelectric-electro-optic effect in lithium niobate on whispering-gallery modes," *Opt. Lett*, vol. 41, pp. 5474–5477, 2016.
[52] A. A. Savchenkov, V. S. Ilchenko, A. B. Matsko, and L. Maleki, "Kilohertz optical resonances in dielectric crystal cavities," *Phys. Rev. A*, vol. 70, 2004, Art. no. 051804(R).
[53] K. Saleh *et al.*, "Phase noise performance comparison between optoelectronic oscillators based on optical delay lines and whispering gallery mode resonators," *Opt. Exp.*, vol. 22, pp. 32158–32173, 2014.
[54] R. M. Nguimdo, K. Saleh, A. Coillet, G. Lin, R. Martinenghi, and Y. K. Chembo, "Phase noise performance of optoelectronic oscillators based on whispering-gallery mode resonators," *IEEE J. Quantum Electron.*, vol. 51, no. 11, Nov. 2015, Art. no. 6500308.
[55] Y. K. Chembo, I. S. Grudinin, and N. Yu, "Spatiotemporal dynamics of Kerr-Raman optical frequency combs," *Phys. Rev. A*, vol. 92, 2015, Art. no. 043818.
[56] G. Lin, S. Diallo, J. M. Dudley, and Y. K. Chembo, "Universal nonlinear scattering in ultra-high Q whispering gallery-mode resonators," *Opt. Exp.*, vol. 24, pp. 14880–14894, 2016.
[57] J. U. Furst *et al.*, "Quantum light from a whispering-gallery-mode disk resonator," *Phys. Rev. Lett*, vol. 106, 2011, Art. no. 113901.
[58] Y. K. Chembo, "Quantum dynamics of Kerr optical frequency combs below and above threshold: Spontaneous four-wave mixing, entanglement, and squeezed states of light," *Phys. Rev. A*, vol. 93, 2016, Art. no. 033820.